

## London Dispersion Interactions



## Do Docking Sites Persist Upon Fluorination? The Diadamantyl Ether-Aromatics Challenge for Rotational Spectroscopy and Theory

María Mar Quesada-Moreno<sup>+, [a]</sup> Pablo Pinacho<sup>+, [a]</sup> Cristóbal Pérez,<sup>[a]</sup> Marina Šekutor,<sup>[c]</sup> Peter R. Schreiner,<sup>[c]</sup> and Melanie Schnell<sup>\*[a, b]</sup>

**Abstract:** Fluorinated derivatives of biological molecules have proven to be highly efficient at modifying the biological activity of a given protein through changes in the stability and the kind of docking interactions. These interactions can be hindered or facilitated based on the hydrophilic/hydrophobic character of a particular protein region. Diadamantyl ether (C<sub>20</sub>H<sub>30</sub>O) possesses both kinds of docking sites, serving as a good template to model these important contacts with aromatic fluorinated counterparts. In this work, an experimental study on the structures of several complexes between diadamantyl ether and benzene as well as a series of fluorinated benzenes is reported to analyze the effect of H→F substitution on the interaction and structure of the resulting molecular clusters using rotational spectroscopy. All experimentally observed complexes are largely dominated by London dispersion interactions with the hydrogen-terminated surface areas of diadamantyl ether. Already single substitution of one hydrogen atom with fluorine changes the preferred docking site of the complexes. However, the overall contributions of the different intermolecular interactions are similar for the different complexes, contrary to previous studies focusing on the difference in interactions using fluorinated and non-fluorinated molecules.

Noncovalent interactions may be subtle, but they play a decisive role in the chemistry of life (ref. [1] and references therein). The surfaces of biological macromolecules, such as proteins or DNA, often present extended hydrophobic areas with polar groups in the inner part.<sup>[2]</sup> In this situation, noncovalent interactions occurring with the surrounding groups may become

the dominating interactions for molecular stabilization.<sup>[3,4]</sup> Within the portfolio of noncovalent interactions, London dispersion (LD) interactions<sup>[5]</sup> have gained attention due to their importance in fine-tuning structural stabilization and thus in chemical reactivity and catalysis.<sup>[1b,3,4]</sup> Intra- or intermolecular LD interactions can further stabilize structures and tip the balance towards a certain class of binding motifs.<sup>[1,6,7]</sup> Detailed computational and experimental studies of systems engaging in LD interactions are important for understanding their role in governing structural arrangements of supramolecular non-polar complexes.<sup>[4,8]</sup> One of the canonical systems used in benchmarking the performance of new quantum-chemical methods is the benzene dimer.<sup>[9]</sup> Benzene's chemical properties can be significantly modified by substitution of hydrogen with halogen atoms, especially with the highly electronegative fluorine. In addition to its large electronegativity, fluorine also has a low polarizability; exchange of hydrogen atoms with fluorine in organic molecules thus results in enhanced bond polarization (C–H vs. C–F bonds). The effect of fluorine substitution on the electronic density in the ring stems from the interplay between inductive and mesomeric effects and is additive with increasing number of fluorine atoms, showing an inversion of the ring electron density from benzene ( $\pi$ -cloud) to hexafluorobenzene ( $\pi$ -hole).<sup>[10]</sup> Such effective reversal of electron density distribution in perfluorinated phenyl rings is a feature readily applied in many fields, ranging from catalysis to bioactive molecules design.<sup>[11]</sup> Fluorination can also alter the physical and chemical properties of proteins and peptides as well as their biological activity, which makes fluorine substitution an expanding research area.<sup>[12]</sup>


The effect of H→F substitution has been extensively studied theoretically<sup>[8,13]</sup> and experimentally in crystal structures (ref. [14] and references therein). As in the case of substituted stilbenes, already partial substitution can alter the crystal pack-


[a] Dr. M. M. Quesada-Moreno,<sup>+</sup> Dr. P. Pinacho,<sup>+</sup> Dr. C. Pérez, Prof. Dr. M. Schnell  
Deutsches Elektronen-Synchrotron (DESY)  
Notkestr. 85, 22607 Hamburg (Germany)  
E-mail: melanie.schnell@desy.de

[b] Prof. Dr. M. Schnell  
Institute of Physical Chemistry, Christian-Albrechts-Universität zu Kiel  
Max-Eyth-Str. 1, 24118 Kiel (Germany)

[c] Dr. M. Šekutor, Prof. Dr. P. R. Schreiner  
Institute of Organic Chemistry, Justus Liebig University  
Heinrich-Buff-Ring 17, 35392 Giessen (Germany)

[\*] These authors contributed equally to this work.

 Supporting information and the ORCID identification numbers for the authors of this article can be found under:  
<https://doi.org/10.1002/chem.202100078>

 © 2021 The Authors. Published by Wiley-VCH GmbH. This is an open access article under the terms of the Creative Commons Attribution Non-Commercial License, which permits use, distribution and reproduction in any medium, provided the original work is properly cited and is not used for commercial purposes.



Part of a Special Collection on Noncovalent Interactions.

ing dramatically.<sup>[14b,c]</sup> However, under the isolated conditions of the gas phase, free of packing effects, there are fewer examples of this type of exchange and its effects. Water complexes with benzene or fluorinated benzene have been used to study the effect of this substitution.<sup>[15,16]</sup> For example, hexafluorobenzene and benzene interact very differently with water. Fluorination leads to a structural rearrangement of the water in the 1:1 complex, going from an O–H... $\pi$  hydrogen bond in benzene-water to an O... $\pi$  linkage in hexafluorobenzene-water. Interestingly, the strength of the interaction was nevertheless found to be almost the same.<sup>[15,16]</sup> In these extreme cases of full substitution, the water molecule is located above the aromatic ring plane. However, in 1:1 complexes of the intermediates tetrafluorobenzene, *p*-difluorobenzene, and fluorobenzene with water, the water molecule sits in-plane to the aromatic ring, stabilized through O–H...F and C–H...O interactions.<sup>[16]</sup>

Here, we investigate the intermolecular interactions between diadamantyl ether (DAE, C<sub>20</sub>H<sub>30</sub>O) and benzene as well as two fluorinated benzenes to explore how a change in the electronic density due to H→F substitution affects the interactions at play and determines the preferred binding site in DAE-aromatics complexes. DAE provides two qualitatively different docking sites—the adamantyl subunits and the partially shielded oxygen atom, so it can be used as a model that resembles macromolecular systems with outer hydrophobic and inner polar groups.

We use high-resolution, high-sensitivity broadband rotational spectroscopy<sup>[17,18]</sup> in the 2–8 GHz region; this low frequency range is optimal for such large aggregates, which have large moments of inertia, thus small rotational constants and low transition frequencies. Rotational spectroscopy offers the possibility to determine the structures of weakly bound complexes in an isolated environment under the cold conditions of a supersonic expansion. Since the molecules in the gas phase are free of crystal packing or solvent effects,<sup>[19]</sup> the experimental results can be compared with the outcome of quantum-chemical computations for benchmarking purposes. Due to the inherent fingerprint character of rotational spectra, structurally related molecules like isomers, diastereomers, conformers, and isotopologues can be easily differentiated.<sup>[6c,20]</sup> To investigate the fluorination effect on the structures of the complexes, a systematic study was performed by increasing the degree of fluorination in the aromatic ring starting with benzene (Figure 1).

We observed rotational spectra of DAE complexed with benzene (C<sub>6</sub>H<sub>6</sub>) (one observed isomer), fluorobenzene (C<sub>6</sub>H<sub>5</sub>F) (one observed isomer), and hexafluorobenzene (C<sub>6</sub>F<sub>6</sub>) (two observed isomers). The results provide relevant information on both ends of the series. It must be noted that despite our efforts no spectra for complexes with C<sub>6</sub>H<sub>5</sub>F were observed.

The outer electron density surface of the DAE monomer is quite homogeneous (Figures 1 and S1). It presents an almost cylindrical shape with convex (“lobes”) and concave (“valleys”) features created by the alkyl hydrogen atoms. The oxygen atom is partially shielded by the two bulky adamantyl moieties, but it influences the electron density in its immediate environment. Hydrogen bonding with the ether oxygen atom, O–

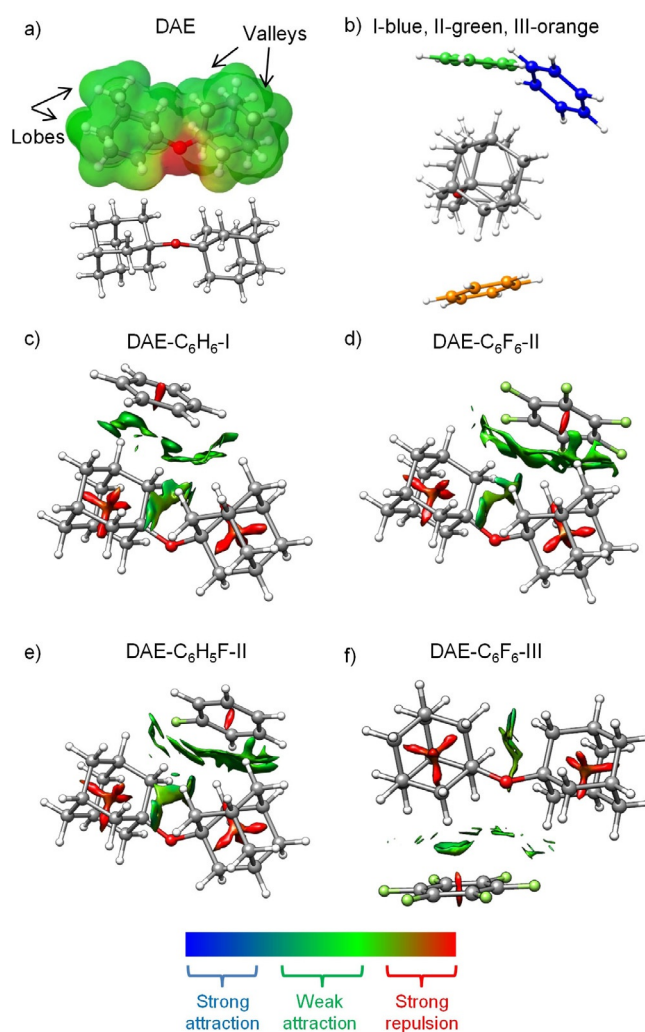


**Figure 1.** (a) The electronic density of DAE, and (b) the most stable positions for the complexes represented for the DAE-C<sub>6</sub>H<sub>6</sub> isomers. (c)–(f) Noncovalent interaction (NCI) analyses for DAE-aromatic ring complexes. Areas in green correspond to low electronic density, while red shows high electronic density. For the NCI, green surfaces represent weak attractive interactions, red indicates repulsion.

H...O, was previously observed to be the main interaction for polar molecules R–OH (R=H, Et, and *t*Bu).<sup>[21]</sup> A conformational search using the GFN-xTB program<sup>[22]</sup> suggested that the aromatic ring can interact with the ether oxygen or with any alkyl group from DAE, resulting in about 15 non-redundant minima for each of the DAE-aromatic systems. During geometry optimization at the B3LYP-D3(BJ)<sup>[23a,b]</sup>/def2-TZVP<sup>[23c]</sup> level of theory, three distinct arrangements turned out to be especially favorable for all the systems. Those positions were labelled as I, II or III to differentiate between the positions of the aromatic ring with respect to DAE (Figures 1 b, S2, and S3). After geometry optimization, no structures with the aromatic ring interacting directly with the ether oxygen, C–H...O or C–F...O, were found among the lowest-energy isomers ( $\Delta E=6.6$  kJ mol<sup>−1</sup> for DAE-C<sub>6</sub>H<sub>6</sub>-O). This is contrary to the complexes with water and several alcohols, which bind to DAE mainly via hydrogen bonding.<sup>[21]</sup> The computed rotational parameters for all the possible complexes in these positions are collected in Tables S1–S5.

In the following, we summarize the rotational spectroscopy analysis for the three DAE-aromatic species and discuss their structures and intermolecular interactions based on the spectroscopic and quantum-chemical results. Portions of the experimental rotational spectra and the experimental and theoretical rotational parameters are collected in the Supporting Information and in Table 1 and Table 2, respectively. The spectra of the observed DAE complexes were too weak (*vide infra*) to observe the singly substituted  $^{13}\text{C}$ - or  $^{18}\text{O}$ -isotopologues in natural abundance, which would have provided us with the experimental structures of the complexes. Thus, we restrict the analysis to structure identification by comparing the experimental rotational constants and the observed types of transitions with the results of quantum-chemical computations. The type of the observed rotational transitions can be particularly useful for the assignment, especially for such large molecular systems. According to the selection rules for asymmetric rotors, such as the complexes studied here, so-called *a*-, *b*-, and *c*-type transitions are allowed. Their strengths depend on the square of the respective dipole-moment components  $\mu_a$ ,  $\mu_b$ , and  $\mu_c$ , which are the projections of the electric dipole moment vector onto the principal axes system. The observation or non-observation of certain types of rotational transitions thus directly provides information on the magnitude of  $\mu_a$ ,  $\mu_b$ , and  $\mu_c$ .

**Table 1.** Experimental rotational parameters for the observed complexes.

	DAE-C <sub>6</sub> H <sub>6</sub> -I	DAE-C <sub>6</sub> H <sub>5</sub> F-II	DAE-C <sub>6</sub> F <sub>6</sub> -II	DAE-C <sub>6</sub> F <sub>6</sub> -III
A [MHz] <sup>[a]</sup>	248.96955(7) <sup>[e]</sup>	216.86266(6)	157.7562(1)	171.150(8)
B [MHz]	172.04887(8)	169.87179(3)	122.9849(1)	109.1306(1)
C [MHz]	120.62305(4)	112.61724(3)	88.2676(2)	83.43218(9)
$\Delta_J$ [kHz]	0.0033(1)	0.00106(2)	0.0032(3)	[0]
$\Delta_{JK}$ [kHz]	0.0834(5)	0.0444(2)	-0.008(1)	0.1467(6)
$\Delta_K$ [kHz]	-0.0673(4)	-0.0327(1)	0.0127(7)	-2.2(1)
$\delta_J$ [kHz]	0.00081(6)	[0] <sup>[f]</sup>	0.0009(1)	[0]
$\delta_K$ [kHz]	-0.0233(4)	0.0184(1)	[0]	[0]
<i>a</i> / <i>b</i> / <i>c</i> <sup>[b]</sup>	n/y/n	y/y/y	n/n/y	y/y/n
<i>N</i> <sup>[c]</sup>	338	904	190	136
$\sigma$ [kHz] <sup>[d]</sup>	5.3	6.0	7.3	8.0

[a] *A*, *B*, and *C* are the rotational constants;  $\Delta_J$ ,  $\Delta_{JK}$ ,  $\Delta_K$ ,  $\delta_J$ , and  $\delta_K$  are the quartic centrifugal distortion constants. [b] *a*, *b*, and *c* are the type of transitions observed (*n*: not observed, *y*: observed). [c] *N* is the number of fitted transitions. [d]  $\sigma$  is the root-mean square deviation of the fit. [e] Standard error in parentheses in units of the last digit. [f] Parameters in square brackets were kept fixed to 0 during the fit.

For DAE-C<sub>6</sub>H<sub>6</sub>, the experimentally observed complex shows only *b*-type rotational transitions, which means that the  $\mu_a$  and  $\mu_c$  values can be assumed to be small. The experimental rotational constants could agree with both isomer I and isomer II, which are computed to be isoenergetic (0.0 and 0.4 kJ mol<sup>-1</sup>, respectively, Tables 1, 2 and S1). We assigned the observed species to DAE-C<sub>6</sub>H<sub>6</sub>-I based on a slightly better agreement of the *B* and *C* rotational constants although *A* seems to agree better with DAE-C<sub>6</sub>H<sub>6</sub>-II (Tables 1, 2 and S1). The *A* rotational constant is usually predicted with less accuracy by quantum-chemical calculations than *B* and *C*. This effect can be especially important in our system due to the elongated shape of DAE and the many possible binding sites for the aromatic partners. Even a slight change in the orientation of the benzene ring can produce a larger change in *A* than in the *B* and *C* rotational constants. The assignment is supported by dipole moment considerations; according to the sizeable  $\mu_c$  value for structure II (0.8 D), we would expect the observation of *c*-type transitions, which were clearly absent in the spectra (Figure S10), corroborating our assignment. We performed a noncovalent interaction (NCI) analysis to illustrate the relevant intermolecular interactions in these complexes.<sup>[24]</sup> The DAE-C<sub>6</sub>H<sub>6</sub>-I complex is stabilized via C–H... $\pi$  and C–H...H–C LD interactions, and the lobe-valley shapes between DAE and the aromatic rings are reproduced (Figures 1 and S4). Additional NCI views and their scatter graphs are provided in Figures S4–S9 in the Supporting Information.

The analysis of the DAE-C<sub>6</sub>H<sub>5</sub>F complex brings up a complication in the assignment. Each of the three potential positions of the aromatic ring (I, II, or III, Figure 1 b) with respect to DAE presents six almost isoenergetic rotamers that only differ in the position of the fluorine atom, denoted as *a*, *b*, *c*, *d*, *e*, and *f*. Those six rotamers have similar rotational constants (Figure S3 and Tables S2–S4) because of the high mass contribution of the DAE moiety. However, the dipole-moment components change substantially, which allows for their differentiation. Experimentally, we observed only one DAE-C<sub>6</sub>H<sub>5</sub>F complex, and it exhibits all three types of rotational transitions (Table 1), corresponding to sizeable  $\mu_a$ ,  $\mu_b$ , and  $\mu_c$  dipole-moment components. Overall, the rotamers belonging to DAE-C<sub>6</sub>H<sub>5</sub>F-II are the lowest-energy ones (Figure S11 and Tables S2–S4). They also show the best agreement with the experimentally determined rotational constants. Among them, DAE-C<sub>6</sub>H<sub>5</sub>F-II-e is the only one that presents dipole-moment components in good concordance with the experimental intensities ( $\mu_a \approx$

**Table 2.** Computed rotational parameters for the complexes discussed (B3LYP-D3(BJ)/def2-TZVP).

	DAE-C <sub>6</sub> H <sub>6</sub> -I	DAE-C <sub>6</sub> H <sub>6</sub> -II	DAE-C <sub>6</sub> H <sub>5</sub> F-II-e	DAE-C <sub>6</sub> F <sub>6</sub> -I	DAE-C <sub>6</sub> F <sub>6</sub> -II	DAE-C <sub>6</sub> F <sub>6</sub> -III
A [MHz] <sup>[a]</sup>	256.0	248.0	220.4	166.3	158.2	173.5
B [MHz]	171.3	175.0	170.5	116.6	124.0	112.9
C [MHz]	121.8	122.2	113.8	86.9	89.0	86.6
$ \mu_a / \mu_b / \mu_c $ [D] <sup>[b]</sup>	0.5/1.4/0.2	0.2/1.0/0.8	1.4/0.9/1.3	0.7/0.7/0.1	0.3/0.3/0.9	0.8/0.7/0.6
$\Delta E_{\text{ZPE}}$ [kJ mol <sup>-1</sup> ] <sup>[c]</sup>	0.0	0.4	0.0	3.3	0.0	1.6

[a] *A*, *B*, and *C* are the rotational constants; [b]  $|\mu_a|$ ,  $|\mu_b|$ , and  $|\mu_c|$  are the absolute values of the dipole moment components; [c]  $\Delta E_{\text{ZPE}}$  are relative energies with respect to the most stable minimum for each system including zero point correction.

$\mu_c > \mu_b$ , see Table 2 and Figure S12). The corresponding NCI analysis shows an almost continuous attraction between DAE and  $C_6H_5F$  (Figures 1 and S6), with  $C-H\cdots\pi$ ,  $C-H\cdots H-C$ , and  $C-H\cdots F$  interactions. Thus, the substitution of just one hydrogen atom with fluorine changes the experimentally observed DAE docking site, from I in the DAE- $C_6H_6$  system to II in the DAE- $C_6H_5F$  complex.

Finally, two complexes are observed for DAE- $C_6F_6$ . The most intense isomer features only *c*-type transitions, and its rotational constants and dipole-moment components agree reasonably well with the lowest-energy isomer DAE- $C_6F_6$ -II (Tables 1 and 2). The interactions of DAE- $C_6F_6$ -II are characterized by an extended surface similar to that of DAE- $C_6H_5F$ -II-e (Figures 1 and S7). Full fluorine substitution thus gives rise to a similar preferred structure as a partial substitution with just one fluorine atom. The spectral features of the second detected DAE- $C_6F_6$  complex show *a*- and *b*-type transitions, but all of them consist of blended lines, as discussed below (Figure S13). As a result, the *A* and *B* rotational constants are highly correlated. The parameters used in the fit are *A* and the linear combination  $(B+C)/2$ , from which the values summarized in Table 1 can be extracted. The good agreement between the experimental and computed rotational constants (Table 2) and the asymmetry parameter  $\kappa$  ( $-0.41$  experimental,  $-0.40$  computed, Table S5) leads us to identify the second DAE- $C_6F_6$  complex as DAE- $C_6F_6$ -III in the experiment. Although  $\mu_c$  is similar to  $\mu_a$  and  $\mu_b$ , no *c*-type transitions were observed. Since the *a*- and *b*-type transitions appear as blended lines, their intensities are enhanced so that we can detect them. It must be noted that, computationally, no real minimum for an O-bound isomer could be obtained for DAE- $C_6F_6$ .

A closer look at the NCI results reveals that for DAE- $C_6F_6$ -II quite localized  $C-H\cdots\pi$  and  $C-H\cdots F$  interactions are present (Figures 1 and S7). DAE- $C_6F_6$ -III shows a more extended interaction surface, in which one of the lone pairs of the oxygen atom could be involved. There is also a clear  $C-H\cdots\pi$  interaction from one DAE hydrogen atom to the center of the  $C_6F_6$  ring.

Symmetry-adapted perturbation theory (SAPT(0)) calculations<sup>[25]</sup> were performed to provide insight into the different binding contributions in each of the DAE complexes. The overall interaction energies are of comparable magnitude for the respective complexes, with the dispersion contribution being the largest by far, around 70% of the overall attractive interaction (see Supporting Information for a discussion of the SAPT results).

At a first glance, the lack of notable structural differences for the complexes between DAE and  $C_6H_6$ ,  $C_6H_5F$ , and  $C_6F_6$ , respectively, is a surprising result. After all, the highly electronegative fluorine present in a polar covalent  $C-F$  bond does not immediately invoke the notion of LD interactions like its  $C-H$  counterpart does. However, fluoro-derivatives are indeed capable of engaging in intermolecular dispersion interactions. For example, the binding interaction of the  $CF_4$  dimer is stronger than the analogous  $CH_4$  dimer and is for the most part a consequence of electron correlation, pointing towards dispersion effects.<sup>[26]</sup> Since attraction between the two  $CF_4$  molecules in a

dimer persists even at larger distances, short range interactions like charge transfer do not appear to be the major source of the pulling effect.<sup>[27]</sup>

Over the years a debate was ongoing whether electrostatic or dispersive factors were predominant in organofluorine systems, and many insights were achieved by considering the benzene/hexafluorobenzene pair. Namely, crystal structures of both  $C_6H_6$  and  $C_6F_6$  revealed an expected herringbone pattern, whereas the  $C_6H_6$ - $C_6F_6$  crystal obtained from the corresponding 1:1 mixture had molecules stacked in alternating columns.<sup>[27,28]</sup> Computational studies demonstrated that even though both dispersion and electrostatic interactions play important roles for the directionality of the overall arrangement, dispersion is still the major source of attraction in the  $C_6H_6$ - $C_6F_6$  complex. As in the case of the  $CF_4$  dimer, the  $C_6H_6$ - $C_6F_6$  complex was computed to have substantial long-range attraction, excluding charge transfer as a governing influence.<sup>[27]</sup> This rationale was extended to other fluorine-containing dimers, with an overall conclusion that the dimer interaction energy grows almost linearly with the number of  $C-F\cdots F$  bonds, dominated by the energetic component ascribed to dispersion, but also noting that the relative orientation of the molecules participating in such bonding affects the bond strength as well.<sup>[29]</sup> It was also found that  $F\cdots F$  electrostatic repulsion, a major concern when considering complexes with spatially close fluorine atoms, was neither large nor influential in its contribution to the total complexation energy.<sup>[28]</sup> Moreover, intermolecular attractions between fluoroaromatics were actually slightly more attractive than those of the hydrogen-containing analogues.

Dunitz convincingly demonstrated that dispersion is by far the most important cohesive contribution for the  $C_6H_6$  and  $C_6F_6$  homodimers as well and that Coulombic energies acting in those homodimers are not strongly destabilizing, as would be expected from a point-charge or quadrupole moment model suggested in the previously mentioned debate.<sup>[30]</sup> Dunitz proposed that for these types of systems dispersion of atoms and molecules can be quantified as a simple ratio of polarizability and volume. Recently, Pollice and Chen further developed this concept by also taking into account linear dimensions of molecules and the spatial distribution of polarizability therein.<sup>[31]</sup> Thus, the volume they used was not molecular but rather an interaction volume, that is, a volume derived from the interaction distance of the atoms. In this way, the dispersion interaction capability of specific atoms in a molecule with respect to a point in space is properly accounted for. Using this principle, they confirmed that dispersion effects in perfluoroalkane dimers originate mainly from interactions between the fluorine atoms. Moreover, perfluoroalkanes have a higher intrinsic ability for intermolecular dispersion than alkanes with equal carbon chain length due to influences of both polarizability and ionization potential, but in practice the overall interaction energies are mostly equal because of unsuitable interaction geometries of perfluoroalkane dimers when compared to analogous alkane dimers. These findings illuminate why the strength of LD interactions remains comparable in intermolecular complexes when introducing fluorine atoms into the parent structures already prone to LD attraction.



Going back to our DAE complexes, the oxygen atom of the DAE is strongly shielded by bulky adamantane subunits, and this prevents direct oxygen-aromatic ring interaction previously observed for smaller ethers, like in complexes of dimethyl ether interacting with a benzene ring or with a hexafluorobenzene ring.<sup>[32]</sup> In the absence of an O $\cdots\pi$  interaction possibility, LD remains the only viable intermolecular interaction in the DAE supramolecular structures under study here, with the hydrocarbon bulk being the starting point in the process of complex formation and spatial orientation. It therefore comes as no surprise that DAE complexes with C<sub>6</sub>H<sub>6</sub>, C<sub>6</sub>H<sub>5</sub>F, and C<sub>6</sub>F<sub>6</sub> are structurally so similar, albeit not identical due to the inherently low directionality of the LD interaction.

In summary, we provide an important new aspect for understanding the complex puzzle of fluorine influence in molecular aggregation. The spectroscopic results focus on the influence of the degree of fluorine substitution on the intermolecular interactions between a model molecule exhibiting both oxygen-terminated and hydrogen-terminated areas and substituted benzene molecules. The observed structures clearly show that these complexes are dominated by LD interactions, where several qualitatively similar binding positions are possible (I, II, and III). The aromatic partners interact mainly with the hydrogen atoms of the DAE methylene groups through dispersive C–H $\cdots\pi$ , C–H $\cdots$ F, and C–H $\cdots$ H–C interactions, and the preferred binding position changes upon partial (C<sub>6</sub>H<sub>5</sub>F) or full (C<sub>6</sub>F<sub>6</sub>) substitution, from I in DAE–C<sub>6</sub>H<sub>6</sub> to II in DAE–C<sub>6</sub>H<sub>5</sub>F and DAE–C<sub>6</sub>F<sub>6</sub>, and to III in DAE–C<sub>6</sub>F<sub>6</sub>. In addition, SAPT(0) computations indicate that H $\rightarrow$ F substitution in the aromatic ring does not substantially change the overall nature of the different contributions to the interaction energies, while the experimentally observed lowest-energy structures change. The computed interaction energies for DAE–C<sub>6</sub>H<sub>6</sub>–I, DAE–C<sub>6</sub>H<sub>5</sub>F–II, DAE–C<sub>6</sub>F<sub>6</sub>–II, and DAE–C<sub>6</sub>F<sub>6</sub>–III are of similar magnitudes.

Since the DAE oxygen atom is partly shielded by two bulky groups, direct electrostatic interactions with the aromatic ring are prevented. The lowest isomer with the aromatic ring interacting with the oxygen atom is 6.6 kJ mol<sup>–1</sup> higher in energy than the global minimum (DAE–C<sub>6</sub>H<sub>6</sub>–O), and no real O-bound minimum could be obtained for DAE–C<sub>6</sub>F<sub>6</sub>. Precluding the possibility of electrostatic attraction between the ether oxygen and the aromatic ring due to DAE size and bulkiness, LD interactions take the mantle of being the governing factor in directing complex formation and spatial arrangement.

Our spectroscopic results at the molecular level in the gas phase are useful for benchmarking theory to help extrapolations to macromolecules with considerable dispersion contributions. As LD interactions grow pairwise additively, this becomes increasingly more important with increasing system size. Model systems like DAE can help create a structural database for various interactions that can dominate in biological systems. In this sense, rotational spectroscopy enables the study of isolated complexes and allows for the analysis of their intrinsic inter- and intramolecular interactions. This makes it an ideal tool to discover which interactions prevail in a chemical environment where different functional groups compete.

## Experimental Section and Computational Details

The rotational spectra were measured using the COMPACT spectrometer<sup>[18]</sup> based on chirped-pulse Fourier transform microwave spectroscopy employing a supersonic molecular jet.<sup>[17]</sup> A 4  $\mu$ s chirped pulse covering the 2–8 GHz frequency range was generated, amplified with a traveling wave tube amplifier (300 W) and broadcast into a high-vacuum chamber. The molecular free induction decay signal was recorded for about 40  $\mu$ s in the time domain and fast Fourier transformed to the frequency domain. A fast-frame setup of 8 chirped pulses per supersonic expansion was performed.<sup>[33]</sup> Around 4 million acquisitions were collected for each of the molecular systems in the time domain and then Fourier transformed. The accuracy in the frequency measurement was estimated to be better than 10 kHz with a resolution power better than 25 kHz. The spectra of all the complexes were analyzed using a semirigid rotor Hamiltonian in the A reduction and the  $I$  representation.<sup>[34]</sup>

Benzene and the different fluorobenzenes were purchased and used without further purification. C<sub>6</sub>H<sub>6</sub> and C<sub>6</sub>F<sub>6</sub> were placed in an external reservoir before the nozzle to seed the carrier gas (Ne at 3 bar of backing pressure) with their vapor. For C<sub>6</sub>H<sub>5</sub>F, a 10 L gas bottle with a final concentration of 0.25% C<sub>6</sub>H<sub>5</sub>F in Ne was prepared and connected to the gas inlet with a backing pressure of 3 bars. Diadamantyl ether is not commercial; it was synthesized and characterized as described in ref. [21]. It was placed in the heatable reservoir of the pulsed nozzle of our spectrometer and heated to ca. 180 °C to increase its vapor pressure and thus the number of molecules in the gas phase. The supersonic jet was formed by the expansion of the gas mixture through a 1 mm diameter nozzle.

The conformational landscape of each complex was explored using the GFN-xTB program.<sup>[22]</sup> The non-redundant structures were optimized using the B3LYP-D3(BJ) dispersion-corrected density functional and the def2-TZVP basis set. The energy values presented herein are zero point corrected relative energies. Structure optimizations including harmonic frequencies were performed using the ORCA package.<sup>[35]</sup> The lowest-energy complexes optimized at the B3LYP-D3(BJ)/def2-TZVP level of theory were used as inputs for the SAPT computations and NCI plots.<sup>[24]</sup> The SAPT analysis was carried out using the PSI4 package.<sup>[25]</sup>

## Acknowledgements

This study was financially supported by the Deutsche Forschungsgemeinschaft (SCHN1280/4-2, project number 271359857, and SCHR597/27-2) in the context of the priority program SPP 1807 “Control of London dispersion interactions in molecular chemistry”. Parts of the computations were performed using the European XFEL and DESY funded Maxwell computational resources operated at Deutsches Elektronen-Synchrotron (DESY), Hamburg, Germany. M.M.Q.M. thanks Fundación Alfonso Martín Escudero for a postdoctoral grant. P.P. and M.Š. thank the Alexander von Humboldt Foundation for postdoctoral fellowships. Open access funding enabled and organized by Projekt DEAL.

## Conflict of interest

The authors declare no conflict of interest.

**Keywords:** diadamantyl ether · dispersion interactions · fluorination · rotational spectroscopy · weakly-bound complexes

- [1] a) P. Hobza, K. Müller-Dethlefs, *Non-Covalent Interactions: Theory and Experiment*, The Royal Society of Chemistry, Cambridge, **2009**; b) J. P. Wagner, P. R. Schreiner, *Angew. Chem. Int. Ed.* **2015**, *54*, 12274–12296; *Angew. Chem.* **2015**, *127*, 12446–12471.
- [2] C. Camilloni, D. Bonetti, A. Morrone, R. Giri, C. M. Dobson, M. Brunori, S. Gianni, M. Vendruscolo, *Sci. Rep.* **2016**, *6*, 28285.
- [3] A. J. Neel, M. J. Hilton, M. S. Sigman, F. Dean Toste, *Nature* **2017**, *543*, 637–646.
- [4] K. E. Riley, P. Hobza, *Acc. Chem. Res.* **2013**, *46*, 927–936.
- [5] a) F. London, *Z. Phys.* **1930**, *63*, 245–279; b) F. London, *Trans. Faraday Soc.* **1937**, *33*, 8b-26.
- [6] a) S. Grimme, *Angew. Chem. Int. Ed.* **2006**, *45*, 4460–4464; *Angew. Chem.* **2006**, *118*, 4571–4575; b) P. R. Schreiner, L. V. Chernish, P. A. Gunchenko, E. Y. Tikhonchuk, H. Hausmann, M. Serafin, S. Schlecht, J. E. P. Dahl, R. M. K. Carlson, A. A. Fokin, *Nature* **2011**, *477*, 308–312; c) S. R. Domingos, C. Pérez, C. Medcraft, P. Pinacho, M. Schnell, *Phys. Chem. Chem. Phys.* **2016**, *18*, 16682–16689; d) D. A. Hewett, S. Bocklitz, D. P. Tabor, E. L. Sibert, M. A. Suhm, T. S. Zwier, *Chem. Sci.* **2017**, *8*, 5305–5318.
- [7] a) M. Goubet, R. A. Motiyenko, F. Réal, L. Margulès, T. R. Huet, P. Asselin, P. Soulard, A. Krasnicki, Z. Kisiel, E. A. Alekseev, *Phys. Chem. Chem. Phys.* **2009**, *11*, 1719–1728; b) P. Pinacho, J. C. López, Z. Kisiel, S. Blanco, *J. Phys. Chem. A* **2019**, *123*, 7983–7990; c) W. Sun, O. P. Sogete, W. G. D. P. Silva, J. van Wijngaarden, *J. Chem. Phys.* **2019**, *151*, 194304.
- [8] S. Ehrlich, J. Moellmann, S. Grimme, *Acc. Chem. Res.* **2013**, *46*, 916–926.
- [9] a) K. C. Janda, J. C. Hemminger, J. S. Winn, S. E. Novick, S. J. Harris, W. Klempere, *J. Chem. Phys.* **1975**, *63*, 1419–1421; b) B. F. Henson, G. V. Hartland, V. A. Ventura, P. M. Felker, *J. Chem. Phys.* **1992**, *97*, 2189–2208; c) E. Arunan, H. S. Gutowsky, *J. Chem. Phys.* **1993**, *98*, 4294–4296; d) R. Podeszwa, R. Bukowski, K. Szalewicz, *J. Phys. Chem. A* **2006**, *110*, 10345–40354; e) B. K. Mishra, S. Karthikeyan, V. Ramanathan, *J. Chem. Theory Comput.* **2012**, *8*, 1935–1942; f) M. Schnell, U. Erlekm, P. R. Bunker, G. von Helden, J.-U. Grabow, G. Meijer, A. van der Avoird, *Angew. Chem. Int. Ed.* **2013**, *52*, 5180–5183; *Angew. Chem.* **2013**, *125*, 5288–5292.
- [10] H. Wang, W. Wang, W. J. Jin, *Chem. Rev.* **2016**, *116*, 5072–5104.
- [11] L. M. Salonen, M. Ellermann, F. Diederich, *Angew. Chem. Int. Ed.* **2011**, *50*, 4808–4842; *Angew. Chem.* **2011**, *123*, 4908–4944.
- [12] a) N. K. Shinada, A. G. de Brevern, P. Schmidtke, *J. Med. Chem.* **2019**, *62*, 9341–9356; b) K. Müller, C. Faeh, F. Diederich, *Science* **2007**, *317*, 1881–1886; c) B. C. Buer, J. L. Meagher, J. A. Stuckey, E. N. G. Marsh, *Proc. Natl. Acad. Sci. USA* **2012**, *109*, 4810–4815; d) M. Salwiczek, E. K. Nyakatura, U. I. M. Gerling, S. Ye, B. Koks, *Chem. Soc. Rev.* **2012**, *41*, 2135–2171; e) J. R. Robalo, L. M. Streacker, D. Mendes de Oliveira, P. Imhof, D. Ben-Amotz, A. Vila Verde, *J. Am. Chem. Soc.* **2019**, *141*, 15856–15868.
- [13] a) S. Tsuzuki, K. Honda, T. Uchimaru, M. Mikami, K. Tanabe, *J. Am. Chem. Soc.* **2002**, *124*, 104–112; b) M. O. Sinnokrot, C. D. Sherrill, *J. Am. Chem. Soc.* **2004**, *126*, 7690–7697; c) K. E. Riley, K. M. Merz, *J. Phys. Chem. B* **2005**, *109*, 17752–17756; d) S. Tsuzuki, T. Uchimaru, M. Mikami, *J. Phys. Chem. A* **2006**, *110*, 2027–2033; e) A. L. Ringer, M. O. Sinnokrot, R. P. Lively, C. D. Sherrill, *Chem. Eur. J.* **2006**, *12*, 3821–3828; f) M. Watt, L. K. E. Hardebeck, C. C. Kirkpatrick, M. Lewis, *J. Am. Chem. Soc.* **2011**, *133*, 3854–3862.
- [14] a) J. D. Dunitz, W. B. Schweizer, *Chem. Eur. J.* **2006**, *12*, 6804–6815; b) R. Mariaca, G. Labat, N.-R. Behrmd, M. Bonin, F. Helbling, P. Eggl, G. Couderc, A. Neels, H. Stoeckli-Evans, J. Hulliger, *J. Fluorine Chem.* **2009**, *130*, 175–196; c) R. Berger, G. Resnati, P. Metrangolo, E. Weber, J. Hulliger, *Chem. Soc. Rev.* **2011**, *40*, 3496–3508; d) M. Cametti, B. Crousse, P. Metrangolo, R. Milani, G. Resnati, *Chem. Soc. Rev.* **2012**, *41*, 31–42.
- [15] a) S. Suzuki, P. G. Green, R. E. Bumgarner, S. Dasgupta, W. A. Goddard, G. A. Blake, *Science* **1992**, *257*, 942–945; b) H. S. Gutowsky, T. Emilsson, E. Arunan, *J. Chem. Phys.* **1993**, *99*, 4883–4893.
- [16] a) K. Brendel, H. Mäder, Y. Xu, W. Jäger, *J. Mol. Spectrosc.* **2011**, *268*, 47–52; b) X. Li, Y. Jin, Q. Gou, Z. Xiz, G. Feng, *J. Chem. Phys.* **2018**, *149*, 164306; c) L. Evangelisti, K. Brendel, H. Mäder, W. Caminati, S. Melandri, *Angew. Chem. Int. Ed.* **2017**, *56*, 13699–13703; *Angew. Chem.* **2017**, *129*, 13887–13891.
- [17] G. G. Brown, B. C. Dian, K. O. Douglass, S. M. Geyer, S. T. Shipman, B. H. Pate, *Rev. Sci. Instrum.* **2008**, *79*, 053103.
- [18] D. Schmitz, V. A. Shubert, T. Betz, M. Schnell, *J. Mol. Spectrosc.* **2012**, *280*, 77–84.
- [19] a) C. Puzzarini, M. Biczysko, V. Barone, L. Largo, I. Peña, C. Cabezas, J. L. Alonso, *J. Phys. Chem. Lett.* **2014**, *5*, 534–540; b) A. A. Fokin, T. S. Zhuk, S. Blomeyer, C. Pérez, L. V. Chernish, A. E. Pashenko, J. Antony, Y. V. Vishnevskiy, R. J. F. Berger, S. Grimme, C. Logemann, M. Schnell, N. W. Mitzel, P. R. Schreiner, *J. Am. Chem. Soc.* **2017**, *139*, 16696–16707; c) S. Blomeyer, M. Linnemannstöns, J. Hendrick Nissen, J. Paulus, B. Neumann, H.-G. Stämmler, N. W. Mitzel, *Angew. Chem. Int. Ed.* **2017**, *56*, 13259–13263; *Angew. Chem.* **2017**, *129*, 13443–13447; d) P. Kraus, I. Frank, *J. Phys. Chem. A* **2018**, *122*, 4894–4901; e) R. Medel, C. Stelbrink, M. A. Suhm, *Angew. Chem. Int. Ed.* **2019**, *58*, 8177–8181; *Angew. Chem.* **2019**, *131*, 8261–8265.
- [20] a) S. T. Shipman, J. L. Neill, R. D. Suenram, M. T. Muckle, B. H. Pate, *J. Phys. Chem. Lett.* **2011**, *2*, 443–448; b) N. A. Seifert, D. P. Zaleski, C. Pérez, J. L. Neill, B. H. Pate, M. Vallejillo-López, A. Lesarri, E. J. Cocinero, F. Castaño, I. Kleiner, *Angew. Chem. Int. Ed.* **2014**, *53*, 3210–3213; *Angew. Chem.* **2014**, *126*, 3274–3277; c) I. Uriarte, S. Melandri, A. Maris, C. Calabrese, E. J. Cocinero, *J. Phys. Chem. Lett.* **2018**, *9*, 1497–1502; d) M. M. Quesada-Moreno, A. Krin, M. Schnell, *Phys. Chem. Chem. Phys.* **2019**, *21*, 26569–26579.
- [21] M. M. Quesada Moreno, P. Pinacho, C. Pérez, M. Šekutor, P. R. Schreiner, M. Schnell, *Chem. Eur. J.* **2020**, *26*, 10817–10825.
- [22] a) S. Grimme, C. Bannwarth, P. Shushkov, *J. Chem. Theory Comput.* **2017**, *13*, 1989–2009; b) C. Bannwarth, S. Ehlert, S. Grimme, *J. Chem. Theory Comput.* **2019**, *15*, 1652–1671.
- [23] a) A. D. Becke, *J. Chem. Phys.* **1993**, *98*, 1372; b) S. Grimme, J. Antony, S. Ehrlich, H. Krieg, *J. Chem. Phys.* **2010**, *132*, 154104; c) F. Weigend, R. Ahlrichs, *Phys. Chem. Chem. Phys.* **2005**, *7*, 3297–3305.
- [24] E. R. Johnson, S. Keinan, P. Mori-Sánchez, J. Contreras-García, A. J. Cohen, W. Yang, *J. Am. Chem. Soc.* **2010**, *132*, 6498–6506.
- [25] a) B. Jeziorski, R. Moszynski, K. Szalewicz, *Chem. Rev.* **1994**, *94*, 1887–1930; b) R. M. Parrish, L. A. Burns, D. G. A. Smith, A. C. Simmonett, A. Eugene De-Prince, E. G. Hohenstein, U. Bozkaya, A. Y. Sokolov, R. D. Remigio, R. M. Richard, J. F. Gonthier, A. M. James, H. R. McAlexander, A. Kumar, M. Saitow, X. Wang, B. P. Pritchard, P. Verma, H. F. Schaefer, K. Patkowski, R. A. King, E. F. Valeev, F. A. Evangelista, J. M. Turney, T. D. Crawford, C. D. Sherrill, *J. Chem. Theory Comput.* **2017**, *13*, 3185–3197.
- [26] M. J. Biller, S. Mecozi, *Mol. Phys.* **2012**, *110*, 377–387.
- [27] S. Tsuzuki, T. Uchimaru, M. Mikami, *J. Chem. Phys.* **2002**, *116*, 3309–3315.
- [28] S. Lorenzo, G. R. Lewis, I. Dance, *New J. Chem.* **2000**, *24*, 295–304.
- [29] R. M. Osuna, V. Hernández, J. T. L. Navarrete, E. D’Oría, J. J. Novoa, *Theor. Chem. Acc.* **2011**, *128*, 541–553.
- [30] J. D. Dunitz, *ChemBioChem* **2004**, *5*, 614–621.
- [31] R. Pollice, P. Chen, *J. Am. Chem. Soc.* **2019**, *141*, 3489–3506.
- [32] a) J. C. Amicangelo, B. W. Gung, D. G. Irwin, N. C. Romano, *Phys. Chem. Chem. Phys.* **2008**, *10*, 2695–2705; b) Y. Geboesa, F. De Proft, W. A. Herrebout, *Chem. Phys. Lett.* **2016**, *647*, 26–30.
- [33] C. Pérez, S. Lobsiger, N. A. Seifert, D. P. Zaleski, B. Temelso, G. C. Shields, Z. Kisiel, B. H. Pate, *Chem. Phys. Lett.* **2013**, *571*, 1–15.
- [34] a) W. Gordy, R. L. Cook, *Microwave Molecular Spectra*, Wiley-Interscience, New York, **1984**; b) J. K. G. Watson, *Vibrational Spectra and Structure a Series of Advances, Vol. 6* (Ed.: J. R. Durig), Elsevier, New York, **1977**, pp. 1–89; c) H. M. Pickett, *J. Mol. Spectrosc.* **1991**, *148*, 371–377.
- [35] a) F. Neese, *WIREs Comput. Mol. Sci.* **2012**, *2*, 73–78; b) F. Neese, *WIREs Comput. Mol. Sci.* **2018**, *8*, e1327.

Manuscript received: January 8, 2021

Accepted manuscript online: January 29, 2021

Version of record online: March 5, 2021